

Article

A Bioorthogonally Synthesized and Disulfide-Containing Fluorescence Turn-On Chemical Probe for Measurements of Butyrylcholinesterase Activity and Inhibition in the Presence of Physiological Glutathione

Ming-Mao Gong ^{1,†}, Chia-Yen Dai ^{2,3,†}, Scott Severance ⁴, Chi-Ching Hwang ⁵, Bo-Kai Fang ¹, Heng-Bo Lin ¹, Chien-Hui Huang ¹, Chi-Wi Ong ⁶, Jeh-Jeng Wang ¹, Pei-Lun Lee ⁷ and Tzu-Pin Wang ^{1,8,*} 

¹ Department of Medicinal and Applied Chemistry, Kaohsiung Medical University, Kaohsiung 80708, Taiwan; orange110129@gmail.com (M.-M.G.); fangken880705@gmail.com (B.-K.F.); gemini810537@gmail.com (H.-B.L.); jennyhuang4128@gmail.com (C.-H.H.); jjwang@kmu.edu.tw (J.-J.W.)

² School of Medicine, College of Medicine, Kaohsiung Medical University, Kaohsiung 80708, Taiwan; d820195@kmu.edu.tw

³ Department of Internal Medicine, Kaohsiung Medical University Hospital, Kaohsiung Medical University, Kaohsiung 80708, Taiwan

⁴ Department of Molecular and Cellular Sciences, Liberty University College of Osteopathic Medicine, Lynchburg, VA 24515, USA; smseverance@liberty.edu

⁵ Department of Biochemistry, Faculty of Medicine, College of Medicine, Kaohsiung Medical University, Kaohsiung 80708, Taiwan; cchwang@kmu.edu.tw

⁶ Department of Chemistry, National Sun Yat-Sen University, Kaohsiung 80424, Taiwan; cong@mail.nsysu.edu.tw

⁷ Chi Mei Hospital, Liouying, Tainan 73657, Taiwan; peilun57@yahoo.com.tw

⁸ Department of Medical Research, Kaohsiung Medical University Hospital, Kaohsiung Medical University, Kaohsiung 80708, Taiwan

* Correspondence: tzupinw@kmu.edu.tw; Tel.: +886-7-312-1101 (ext. 2756); Fax: +886-7-312-5339

† Authors contributed equally to this study.

Received: 19 September 2020; Accepted: 9 October 2020; Published: 12 October 2020



Abstract: Butyrylcholinesterase (BChE) is a biomarker in human blood. Aberrant BChE activity has been associated with human diseases. Here we developed a fluorescence resonance energy transfer (FRET) chemical probe to specifically quantify BChE activity in serum, while simultaneously discriminating against glutathione (GSH). The FRET chemical probe **11** was synthesized from a key trifunctional bicyclononyne *exo*-**6** and derivatives of 5-(2-aminoethylamino)-1-naphthalenesulfonic acid (EDANS) and 4-[4-(dimethylamino)phenylazo]benzoic acid (DABCYL). EDANS fluorescence visualization and kinetic analysis of **11** in the presence of diverse compounds confirmed the outstanding reactivity and specificity of **11** with thiols. The thiol-dependent fluorescence turn-on property of **11** was attributed to a general base-catalyzed S_N2 nucleophilic substitution mechanism and independent of metal ions. Moreover, all thiols, except GSH, reacted swiftly with **11**. Kinetic studies of **11** in the presence of covalently modified GSH derivatives corroborated that the steric hindrance of **11** imposing on GSH was the likely cause of the distinguished reactivity. Since GSH commonly interferes in assays measuring BChE activity in blood samples, the **11**-based fluorescent assay was employed to directly quantify BChE activity without GSH interference, and delivered a linear range of 4.3–182.2 U L⁻¹ for BChE activity with detection limit of 4.3 U L⁻¹, and accurately quantified serum BChE activity in the presence of 10 μM GSH. Finally, the **11**-based assay was exploited to determine K_i of 5 nM for tacrine inhibition on BChE catalysis. We are harnessing the modulated characteristics

of **6** to synthesize advanced chemical probes able to more sensitively screen for BChE inhibitors and quantify BChE activity in serum.

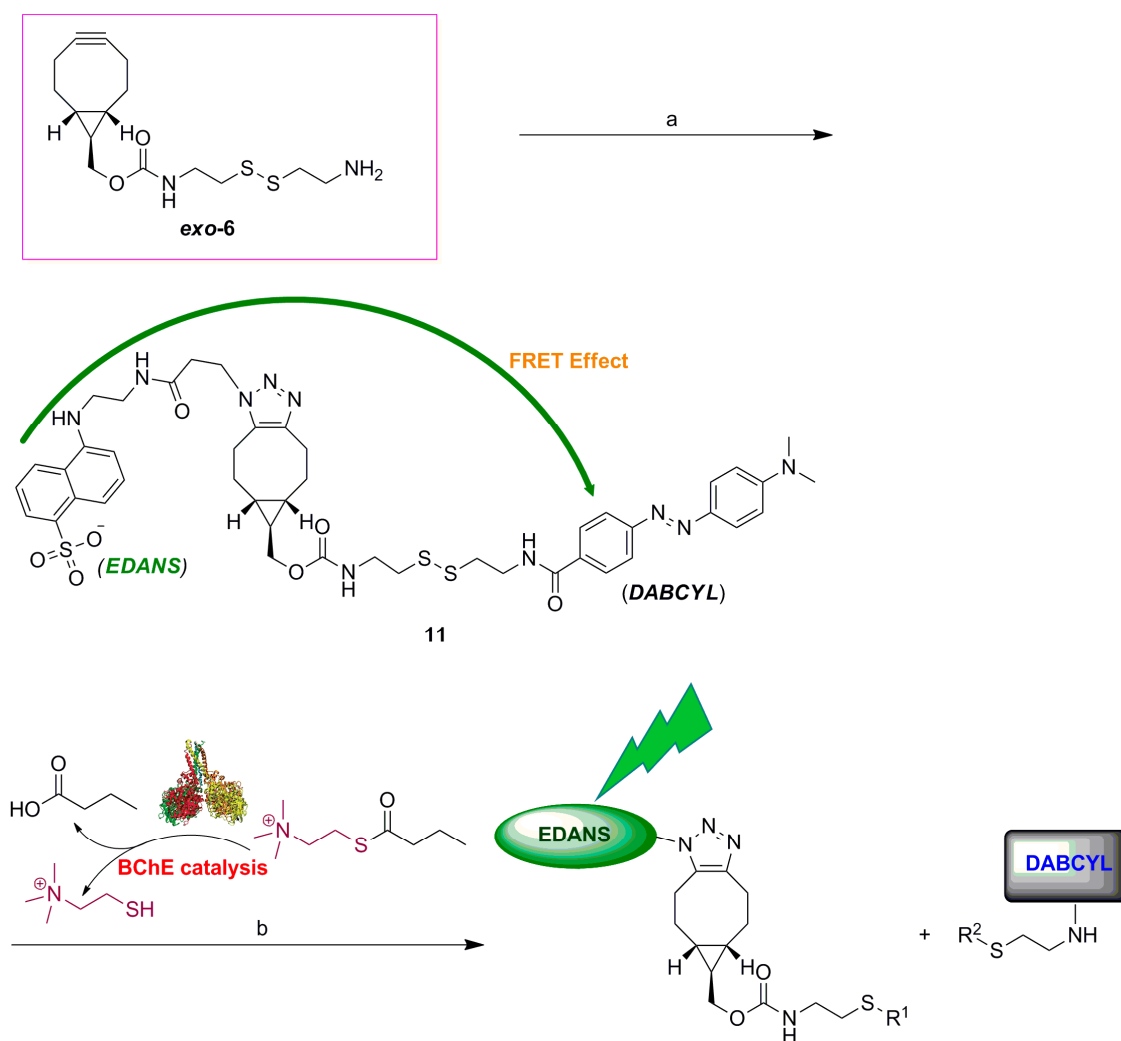
Keywords: fluorescence; disulfide; chemical probe; bioorthogonal; bicyclononyne; glutathione; butyrylcholinesterase; serum; inhibitors

1. Introduction

Butyrylcholinesterase (BChE; EC 3.1.1.8) is ubiquitous in blood plasma and the major cholinesterase (ChE) in human serum. BChE hydrolyzes many different bioactive esters, including acetyl(thio)choline, butyryl(thio)choline, esters in plant-based foods, ester-containing drugs that act at the neuromuscular junctions, and ghrelin, an esterified neuropeptide hormone [1–3]. Aberrant activity of BChE has been closely associated with a range of human disorders such as diabetes, cardiovascular disease, metabolic syndrome, hepatocellular carcinoma, chronic liver diseases, postoperative delirium, and poisoning with organophosphates and metals. BChE has been shown to be critical to the development and progression of diseases [4–8], including Alzheimer's [2,9–15]. Detecting changes in BChE activity in the serum can facilitate reliable and straightforward diagnoses of disease states [1–3,16–19]. BChE levels in human blood have the potential to be a useful biochemical marker [2,4–8,12,13,20–24]. However, a limited number of methods have been developed to measure BChE activity and inhibition, in sharp contrast to the diverse assays available for that of the closely related ChE acetylcholinesterase (AChE; EC 3.1.1.7) [9,25]. Thus, there is an urgent need for medical facilities to have straightforward and accurate techniques to quantify BChE activity.

Several electrochemical [26–28], immunological [29], and mass spectrometric [30] detection methods have been developed to quantify BChE activity. However, BChE catalysis and inhibition are typically determined by using spectroscopic methods, such as colorimetric and fluorometric analysis. Among the spectroscopic methods, Ellman's colorimetric detection method is the most widely used assay for the measurement of BChE activity, as it is relatively simple and can be adapted for high-throughput analysis [31,32]. Ellman's method takes advantage of BChE catalysis to hydrolyze a thiocholine ester substrate to produce thiocholine (TCh), which, in turn, reacts with the disulfide compound 5,5'-dithiobis(2-nitrobenzoic acid) (DTNB) to yield the yellow 5-thio-2-nitrobenzoic acid product with strong absorption at 412 nm. However, the effectiveness of Ellman's method is diminished by the instability of reagents and significant interference from naturally occurring serum biomolecules. One such interfering molecule is glutathione (GSH), a thiol-containing compound abundant in healthy human plasma ($2.09 \pm 1.15 \mu\text{M}$) [33] and capable of reacting with DTNB. Other colorimetric assays that have been developed to overcome interference problems have met with limited success [34–37].

Fluorometric analysis has the potential to improve sensitivity and to lower interference in BChE activity assays. Several fluorogenic methods have been used to measure BChE activity in standard buffer solutions and blood samples [9,15,38–47]. Unfortunately, none of the analytical methods described directly and accurately quantify BChE in the presence of GSH in samples. Thus, there is a demand for a simple and selective BChE assay based on novel and benign fluorescence reagents. Consequently, we were motivated to harness biocompatible and bioorthogonal chemistry to develop sensitive fluorescence resonance energy transfer (FRET) chemical probes, such as **11** (Scheme 1), capable of specifically quantifying BChE activity in human blood samples, while simultaneously discriminating against GSH.



Scheme 1. Synthesis of the FRET chemical probe **11** from *exo-6* and the use of **11** to quantitatively analyze inhibition and activity of BChE. (a) **10**, *N*-succinimidyl 4-[4-(dimethylamino)phenylazo]benzoate (DABCYL NHS ester), *N,N*-diisopropylethylamine (DIPEA), dimethylformamide (DMF), room temperature (rt); (b) phosphate buffer (PB), 37 °C. Thiocholine (TCh) was one of the products of BChE catalysis and is highlighted in pink. The thiolate of TCh later participated in nucleophilic attack on the disulfide bond in **11** to obliterate the FRET effect and to liberate the EDANS fluorescence. R^1 and R^2 , H, or the thiolate of TCh.

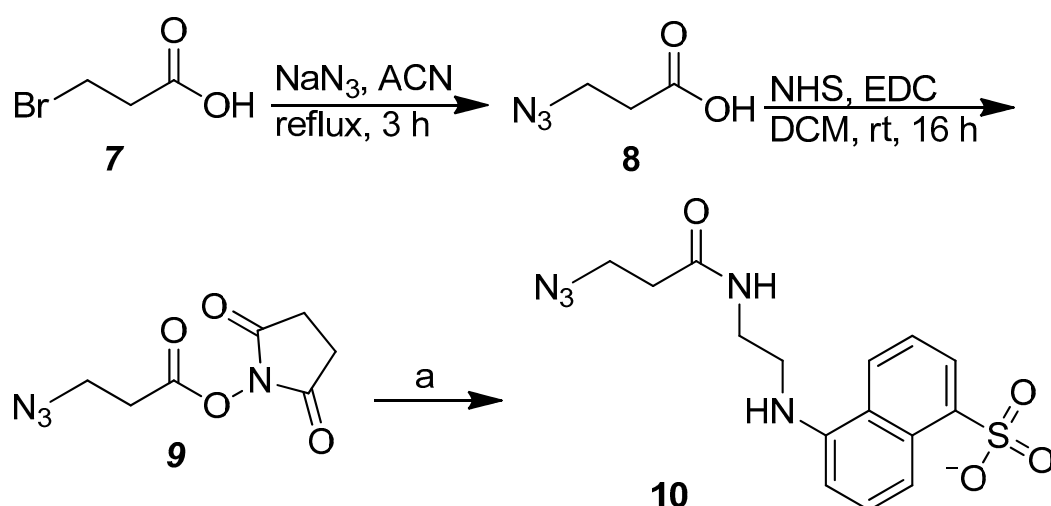
In the current study, we successfully synthesized the novel FRET chemical probe **11** capable of accurately quantifying BChE activity in serum, while simultaneously demonstrating a discriminative reactivity toward GSH. The FRET chemical probe **11** was effectively synthesized from a key disulfide-containing bicyclononyne, *exo-6*, a derivative of 5-(2-aminoethylamino)-1-naphthalenesulfonic acid (EDANS), and a derivative of 4-[4-(dimethylamino)phenylazo]benzoic acid (DABCYL), utilizing a one-pot synthesis strategy, including the bioorthogonal copper-free strain-promoted azide-alkyne cycloaddition (SPAAC) reaction [48]. The presence of the EDANS and DANCYL chromophores and their expected FRET effect in **11** was corroborated by UV-Vis and fluorescence spectroscopy studies. Direct fluorogenic visualization of EDANS fluorescence and determination of pseudo-first-order (k_1) and second-order rate constants (k_2) for reactions involving **11** and various compounds with or without a thiol group confirmed a rapid response, a high reactivity, and a specificity of **11** toward thiol compounds. Titration studies of the reaction between **11** and DL-dithiothreitol (DTT) at several pH levels provided the evidence that the thiol-dependent fluorescence turn-on property of **11** was catalyzed by general bases to liberate the corresponding thiolate able to nucleophilically attack the disulfide bond in **11** and

was mostly inert to the presence of metal ions. Additionally, all thiol-containing reactants, except GSH, swiftly reacted with **11** to increase levels of EDANS fluorescence. The distinguishing reactivity of **11** toward GSH was explicated by kinetic analysis of the **11** reactions in the presence of covalently modified GSH derivatives which shed light on the importance of the steric structure of **11** to prevent GSH from effectively accessing and reacting with it. The **11**-based fluorescent assay was further employed to directly quantify BChE activity in samples without GSH interference, provide a broad linear detection range of BChE activity with low limit of detection (LOD), and to accurately determine BChE activity in serum from healthy humans in the presence of a physiological concentration of GSH. Moreover, the **11**-based assay effectively quantified the inhibitory effect of tacrine, a well-known cholinesterase inhibitor, on BChE catalysis [15,40]. Thus, the innovative FRET chemical probe **11** can directly and accurately determine activity of BChE catalysis and the effects of BChE inhibitors as a function of released EDANS fluorescence in samples without interference from GSH. Moreover, the trifunctional and modulated characteristics of the bicyclononynes **6** will be invaluable reagents to facilitate synthesis of advanced chemical probes for more effective discovery of BChE inhibitors as pharmaceutical agents and more sensitive quantification of BChE activity in serum in clinical settings.

2. Results and Discussion

2.1. Synthesis of the FRET Chemical Probe **11**

The FRET chemical probe **11** (Scheme 1) was synthesized from *exo-6*, a crucial disulfide-containing bicyclononyne able to engage in bioorthogonal copper-free SPAAC reactions [48]. Synthesis of *exo-6* was started with **1**; five sequential reactions yielded **6** (Supplementary Materials Scheme S1) [48]. It is noted that we successfully separated and purified the diastereomeric *exo-2* and *endo-2* by using a straightforward hexane/Et₂O system and acquired both products with good yield. The new hexane/Et₂O system for the purification of *exo-2* and *endo-2* is clearly more amiable to scientists than the previously reported EtOAc/heptane system for the same purification [48]. In addition, we overcame the solubility problem of cystamine in organic solvents and carried out the amidation reaction between **5** and cystamine to produce the highlighted key compounds *exo-6* and *endo-6*. The bicyclononynes **6** could participate in the bioorthogonal and biocompatible SPAAC reaction, an invaluable tool in chemical and biomedical research. The trifunctional nature of **6** also enabled us to modulate the cystamine moiety by incorporating a FRET donor on one side and a FRET acceptor on the other side, and to synthesize fluorescence chemical probes with diverse structures and tunable properties in one-pot reactions. Since the allowed distance between a FRET donor–acceptor pair is 10–100 Å [49] and an extended cystamine is not longer than 30 Å [50], **6** had the appropriate structure to be developed as a group of fluorescence chemical probes. We employed the EDANS–DABCYL pair in this study because the maximum Förster radius for the EDANS–DABCYL pair is 33 Å. In addition, we exploited the availability of the *exo-6* in the **11** synthesis reaction because we always obtained more *exo-2* (76%) than *endo-2* (24%) in the synthesis of **2**. The FRET chemical probe **11** was thus synthesized from a one-pot reaction of *exo-6*, **10** (an azido EDANS; Scheme 2), and DABCYL NHS ester with reasonably good yield (48%) by the simultaneous SPAAC and amidation reactions in the same reaction milieu.



Scheme 2. Synthesis of the azido EDANS derivative (10). Compounds 8 and 9 were synthesized by the previously reported methods [51]. (a) EDANS, DIPEA, rt, DMF.

2.2. FRET and Fluorogenic Properties of the FRET Chemical Probe 11

The afforded FRET chemical probe **11** was initially characterized by UV–Vis spectrophotometry to demonstrate the perturbation of the EDANS (λ_{max} , ~250 nm) and DABCYL (λ_{max} , ~480 nm) absorption due to the proximity of the chromophore moieties in the compound (Supplementary Materials Figure S1). The result was consistent with our previous observation that short distance between a fluorophore and a quencher molecule would facilitate direct electronic interaction of the fluorophore-excited state with the quencher and alter visible absorption properties of the fluorophore–quencher pair [52]. The presence of FRET in **11** was corroborated when reacting **11** with DTT in PB (Figure 1A). Moreover, the FRET quenching of the EDANS fluorescence in **11** was rapidly and completely obliterated within 15 min, suggesting that **11** promptly responds to the presence of appropriate thiol-containing compounds. The fluorogenic properties of **11** in the presence of various compounds with or without a thiol group (Supplementary Materials Figure S2 and Scheme S2) again confirmed the rapid thiol-responsive reactivity of **11** and the potential of **11** to be an effective FRET chemical probe for detection of thiols. Clearly, all thiol-containing reactants, except GSH, were able to swiftly react with **11** and to increase levels of EDANS fluorescence. The reactivity preference of **11** was also consistent with the pseudo-first-order rate constants (k_1) for the reactions (Figure 1B and Supplementary Materials Figure S3). Each of the qualitative and quantitative measurements of the **11** reactions demonstrated that DTT was the most effective of the studied compounds in deterring the FRET effect in **11** and liberating the EDANS fluorescence (Figure 1B and Supplementary Materials Figures S2 and S3).

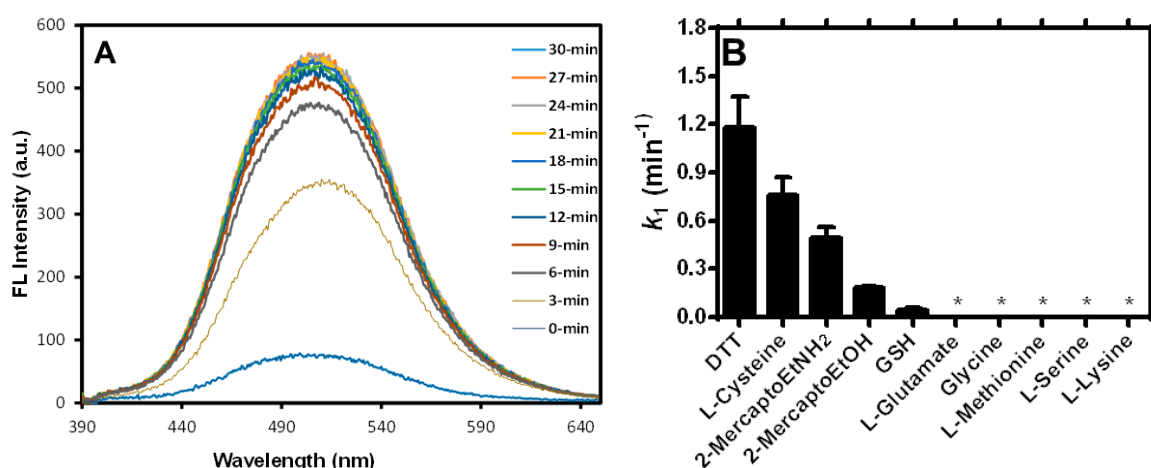


Figure 1. Release of EDANS fluorescence by **11** when reacting with thiol-containing compounds. (A) The time-dependent increase in EDANS fluorescence (FL intensity) in a reaction of **11** (25 μM) with DTT (50 mM). (B) Differential reactivity of **11** toward reactants as demonstrated by the pseudo-first-order rate constants k_1 of the reactions. Please see Materials and Methods for the details. Each reactant was analyzed four times in order to acquire the averaged k_1 values and standard deviation (the error bar). The symbol * indicates that **11** had no detectable reactivity so that values of averaged k_1 and standard deviation could not be determined; 2-MercaptoEtNH₂, 2-aminoethanethiol; 2-MercaptoEtOH, 2-mercaptoethanol.

2.3. Study of the Fluorogenic Reaction Mechanism of **11** with DTT

Kinetic analysis of the reaction between a constant **11** concentration (25 μM) and various [DTT] shed light on the mechanism of the reaction. We determined k_1 values of the reactions of 25 μM of **11** in the presence of different DTT concentrations and plotted values of k_1 vs. [DTT], to obtain a straight line (Figure 2A). This suggested that the **11**-DTT reaction is overall second-order, first-order to **11**, first-order to DTT with the second-order rate constant k_2 of the reaction to be 0.11 $\text{M}^{-1} \text{s}^{-1}$ as calculated from the slope of the line. The observed results supported a S_N2 nucleophilic substitution reaction mechanism in which rapid deprotonation of DTT was followed by the rate-limiting nucleophilic attack of the corresponding thiolate on the disulfide bond in **11** to cleave the disulfide bond and to release the EDANS fluorescence (Supplementary Materials Scheme S2).

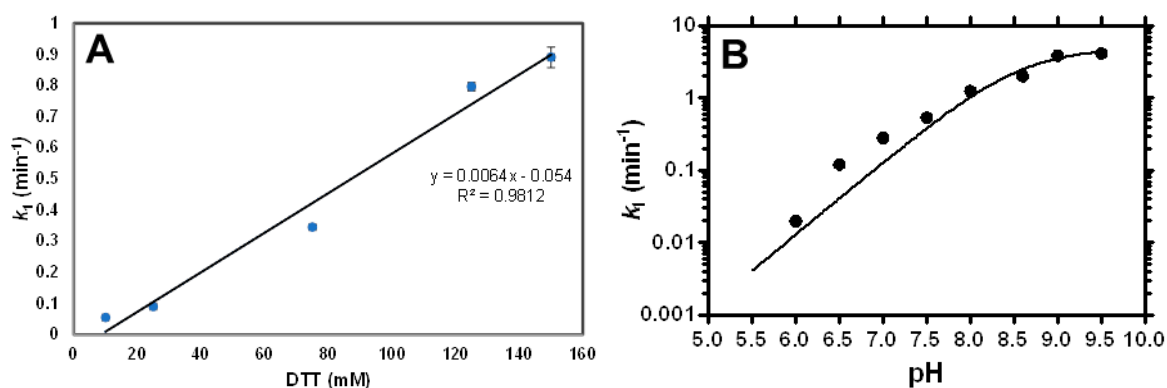


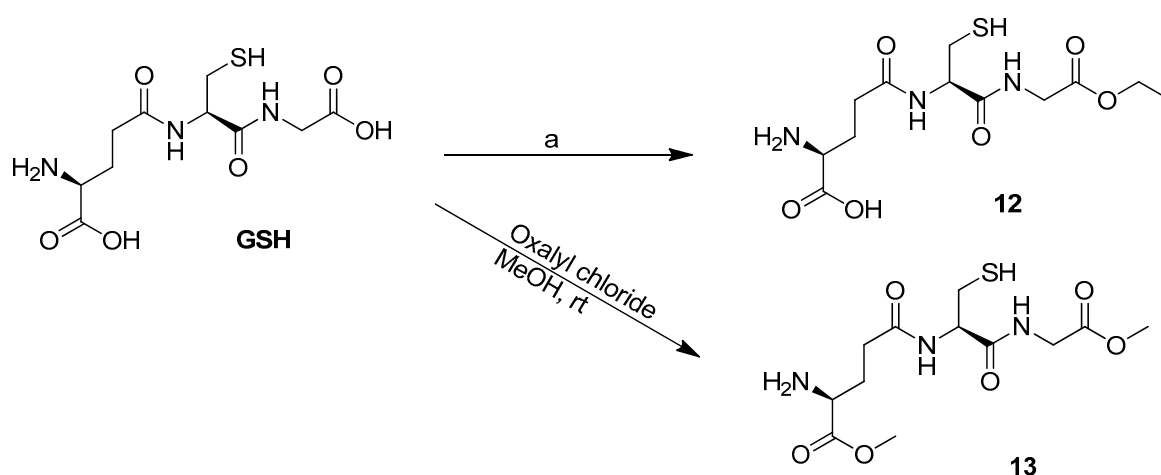
Figure 2. Titration studies to determine the reaction mechanism of **11** with DTT. (A) Kinetic analysis of [DTT] titration on the **11**-DTT reaction was performed in the presence of 25 μM of **11**. (B) Kinetic analysis of pH titration on the **11**-DTT reaction was carried out in the presence of 25 μM of **11** and 50 mM of DTT, while varying pH and/or buffers. Please see Materials and Methods for the details.

A survey of pH and metal ion effects on the **11**-DTT reaction provided additional insight into the reaction mechanism. We first obtained k_1 for the reactions between 25 μM of **11** and 50 mM of DTT in the presence of differing pH and/or buffers. The pH titration results were plotted (Figure 2B) and unequivocally showed incremental changes of k_1 values, while changing the pH of buffers from acidic to alkaline. Moreover, k_1 approximately plateaued at pH 9.5, clearly demonstrating characteristics of general base catalysis to accelerate the **11**-DTT reaction. In addition, the titration study allowed us to determine the $\text{p}K_{\text{a}1}$ of DTT to be 8.6 ± 0.1 , a value being rather consistent with the previously reported 9.2 [53]. Moreover, kinetic studies of reactions in the presence of 25 μM of **11**, 50 mM of DTT, and 1 mM in the studied metal ions indicated that only Cu(II) and Fe(III) showed inhibitory ability on the **11**-DTT reaction (Supplementary Materials Figure S4). For the **11**-DTT reactions containing Co(II) or Ni(II), we found that the two cations formed complexes with **11** and precipitated out of solution to render kinetic analysis of the reactions impractical. Overall, the second-order **11**-DTT reaction is characterized by a general base catalysis with $\text{S}_{\text{N}}2$ nucleophilic substitution reaction mechanism and is not interfered with by metal ions prevalent in biological fluids, such as blood.

2.4. Deciphering the Ability of **11** to Discriminate Against Reactions with GSH

Figure 1B and Supplementary Materials Figures S2 and S3 reveal the peculiar reactivity of **11** toward GSH. Unexpectedly, EDANS fluorescence was almost completely absent in the presence of GSH in phosphate buffer saline (PBS) (Sample 3 in Supplementary Materials Figure S2); and **11** moderately reacted with GSH, judging by the k_1 value for GSH (0.045 min^{-1}), which was approximately one-thirtieth of that for DTT (1.18 min^{-1} ; Figure 1B). The tripeptide GSH contains a Cys residue, and we anticipated it would have a k_1 value comparable to that of Cys, 0.76 min^{-1} . The chemical probe **11** apparently has a unique intrinsic ability to differentiate and rapidly react with most thiol-containing compounds, while remaining rather unreactive to GSH during a similar reaction time of 15–30 min. We thus decided to elucidate the origin of the distinctive reactivity of **11** for GSH.

We first determined that the electrostatic repulsion between **11** and GSH is unlikely the cause of a rather low k_1 because **11** carries a net zero charge at neutral pH. We then turned attention to the steric structure of **11** and reasoned that steric hindrance of **11** imposed on GSH could be the driving force to prevent the corresponding thiolate of GSH from nucleophilically attacking the disulfide bond in **11**. In order to explore the importance of steric effects on the **11**-GSH reaction, we synthesized two GSH derivatives: a monoethyl ester derivative **12** and a dimethyl ester derivative **13** (Scheme 3). Both **12** and **13** were exploited to substitute for GSH in the kinetic analysis of the reactions with **11**. To our surprise, the formation of a monoethyl ester of GSH, i.e., **12**, was bulky enough to abolish its reaction with **11**, to render no detection of released EDANS fluorescence, and to afford k_1 essentially to be zero (Supplementary Materials Figure S5). In contrast, use of the dimethyl ester of GSH **13** in the kinetic analysis of the reaction with **11** provided a k_1 value comparable to that for the **11**-GSH reaction. Clearly, replacement of a methyl group with an ethyl group in GSH enhanced the steric obstruction of **11** so overtly that it completely annihilated the reaction with **12**. Consequently, the steric hindrance of **11** experienced by GSH is the plausible explanation for the rather sluggish k_1 of 0.045 min^{-1} in the **11**-GSH reaction.



Scheme 3. Synthesis of the GSH derivatives (**12** and **13**). Compound **13** was synthesized before [54].
(a) H_2SO_4 , EtOH, rt.

GSH, which is found naturally and abundantly in human blood, commonly interferes in assays used to measure BChE activity in blood samples. Therefore, we believed that **11** could be employed to directly and accurately quantify BChE activity in blood samples, without interference from GSH (Scheme 1).

2.5. GSH not a Source of Interference in the **11**-Based Fluorescence Turn-On Assay for Measuring BChE Activity

It became apparent that the **11**-based assay had the potential to directly and accurately measure BChE activity when it was qualitatively demonstrated that **11** reacted specifically with only the catalytic reaction product TCh, in the presence of BTCh and BChE (Figure 3A). Moreover, the reaction between **11** and TCh was clearly unaffected by the presence of a physiological GSH concentration of $50 \mu\text{M}$. Quantitative analysis of the BChE-BTCh-**11** catalytic system also justified the use of **11** for the accurate detection of BChE activity, even in the presence of physiological levels of GSH (Figure 3B and Supplementary Materials Figure S6). Fluorometric studies of the BChE-BTCh-**11** catalytic system demonstrated that the presence of GSH did not affect the increased levels of EDANS fluorescence contributed by BChE activity (Supplementary Materials Figure S6A). The time–fluorescence curves and enzyme activities of the BChE-BTCh-**11** reaction were almost identical in the presence or absence of $50 \mu\text{M}$ GSH (the initial velocities v_i : $11.7 \pm 0.7 \text{ min}^{-1}$ vs. $10.8 \pm 1.5 \text{ min}^{-1}$, respectively) (Figure 3B) and substantiated the notion that the presence of $2.09 \pm 1.15 \mu\text{M}$ of GSH in healthy human plasma [33] is unlikely to interfere with accurate detection of the BChE activity in blood samples by the **11**-based assay. Moreover, even the presence of 50 mM of GSH had no effect on the enzymatic progression of the BChE-BTCh-**11** catalytic system (Supplementary Materials Figure S6B). Thus, the chemical probe **11** has the critical properties necessary for a quick, sensitive, and specific quantification of the BChE activity in human blood samples.

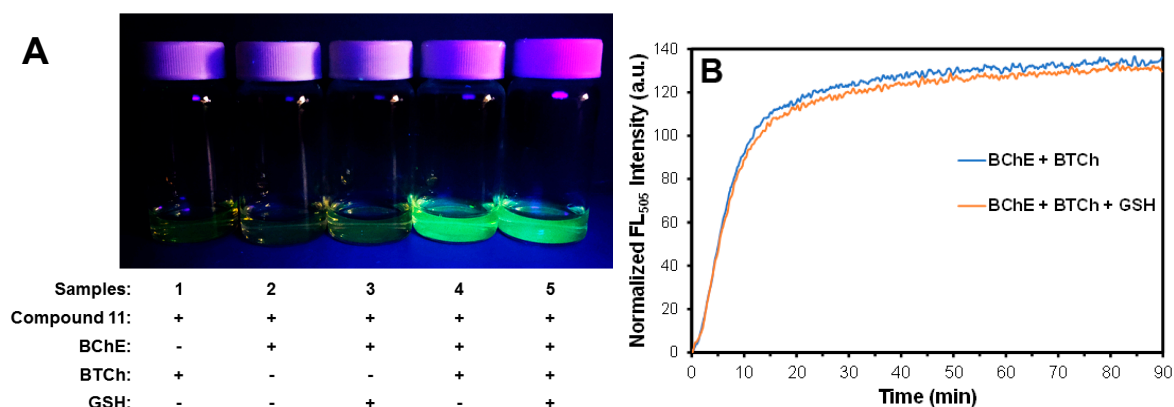


Figure 3. Using the chemical probe **11** for accurate determination of BChE activity in the presence of a physiological concentration of GSH. Each vial contained 25 μM of **11** in PB and various combinations of BChE (182 U L^{-1}), BTCh (5 mM), or GSH (50 μM). The reactions were carried out at rt or 37°C for 90 min, and (A) was visualized by UV lamp illumination (365 nm) or (B) was monitored spectrofluorometrically. In (B), the normalized fluorescent (FL) intensity at 505 nm for each result was acquired by subtracting a background FL₅₀₅ intensity of **11** from the original FL₅₀₅ intensity data.

2.6. Direct and Accurate Determination of BChE Activity in Human Serum by the Fluorescence Turn-On Assay Based on **11**

Demonstration of the **11**-based assay to accurately quantify BChE activity in samples in the presence of GSH (Figure 3 and Supplementary Materials Figure S6) encouraged us to employ the TCh-responsive and EDANS fluorescence-releasing properties of **11** for correct determination of BChE activity in human blood samples. We began with kinetic analysis of time-dependent fluorescence turn-on of **11** in the presence of equine BChE standards, with different activity, to acquire the corresponding values of v_i . Linear regression analysis of BChE activity vs. v_i showed that the **11**-based assay provided a linear calibration curve with a slope m of 0.062 and a good linear detection range of $4.3\text{--}182.2 \text{ U L}^{-1}$ (Figure 4A). LOD of BChE activity by the **11**-based assay was calculated to be 4.3 U L^{-1} , according to the equation of $\text{LOD} = 3s_b/m$ in which the standard deviation s_b of 0.0878 was determined from three blank reactions. The LOD of the **11**-based assay was compared with existing optical methods for BChE activity quantification (Supplementary Materials Table S1) and was explicitly shown to be the only fluorescent chemical probe for BChE analysis able to deliver both low LOD and a broad linear detection range. In addition, even though the **11**-based assay was less sensitive than most nanoprobe-based BChE assays, judged by the LOD values in Supplementary Materials Table S1, our assay for BChE activity determination generally conveyed a linear range that was broader than those based on fluorescent nanoparticle probes.

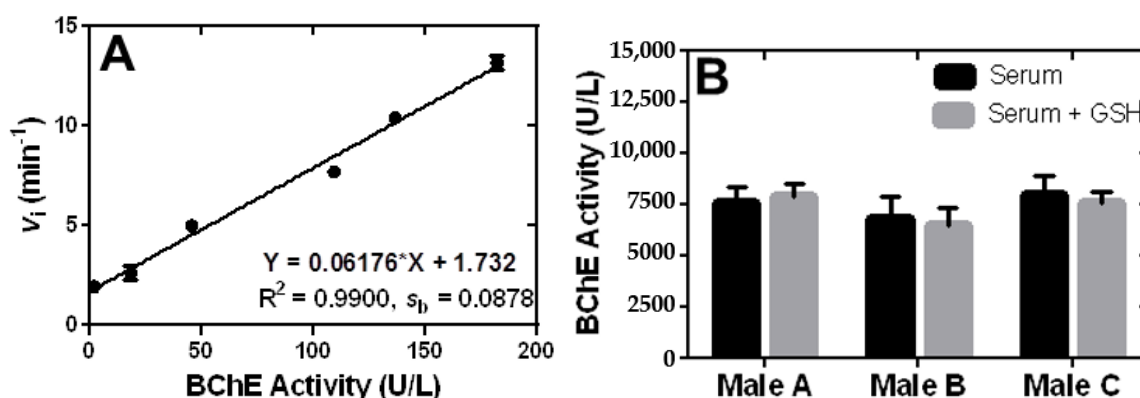


Figure 4. The **11**-based assay for determination of BChE activity in biological samples. (A) BChE standards obtained from equine serum were analyzed by the **11**-based analysis to afford the linear regression calibration curve of BChE activity vs. v_i and to give LOD of 4.3 U L^{-1} and the linear detection range of $4.3\text{--}182.2 \text{ U L}^{-1}$. (B) Serum samples from three healthy males were measured for BChE activity by the **11**-based assay in the presence or absence of spiked $10 \mu\text{M}$ GSH.

The calibration curve in Figure 4A was exploited to determine BChE activity of whole blood and serum samples from three healthy males. None of the whole blood samples provided a fluorescence change to allow v_i determination by the **11**-based analysis (results not shown). The same **11**-based assay, however, successfully quantified BChE activity in the serum samples (Figure 4B) and provided the average BChE activity of $7460 \pm 597 \text{ U L}^{-1}$, which is within the normal physiological range of BChE activity, $5900\text{--}13,200 \text{ U L}^{-1}$ [35]. Moreover, the serum samples spiked with $10 \mu\text{M}$ GSH resulted in BChE activity values not significantly different from those without spiked GSH. This demonstrated that the fluorescence turn-on assay based on **11** is well calibrated to directly and accurately determine BChE activity in serum samples in the presence of physiological GSH concentrations.

2.7. The **11**-Based Fluorescence Assay for Kinetic Analysis of BChE Inhibition

The fluorescence turn-on analysis based on **11** further explicated the potential to measure the inhibition of BChE catalysis and to screen BChE inhibitors. Here we studied the inhibition effect of tacrine on BChE reaction by the **11**-based assay. Tacrine is a well-known cholinesterase inhibitor, which inhibits BChE catalysis by a competitive mechanism [15,40]. We were pleased to observe that the inhibitory assay based on **11** was able to detect gradual decrease of v_i with increasing tacrine concentrations (Figure 5A and Supplementary Materials Figure S7). Kinetic analysis of the tacrine inhibition of BChE catalysis allowed us to acquire a Dixon plot (Figure 5B), which was employed to estimate the K_i value of 5 nM , a result very close to the K_i value of $8.17 \pm 1.17 \text{ nM}$ determined by Ellman's method [15,40]. These results demonstrate that the **11**-based fluorescence assay is well positioned to provide the platform for discovery of novel BChE inhibitors under moderate conditions crucial to the diagnosis and treatment of human diseases.

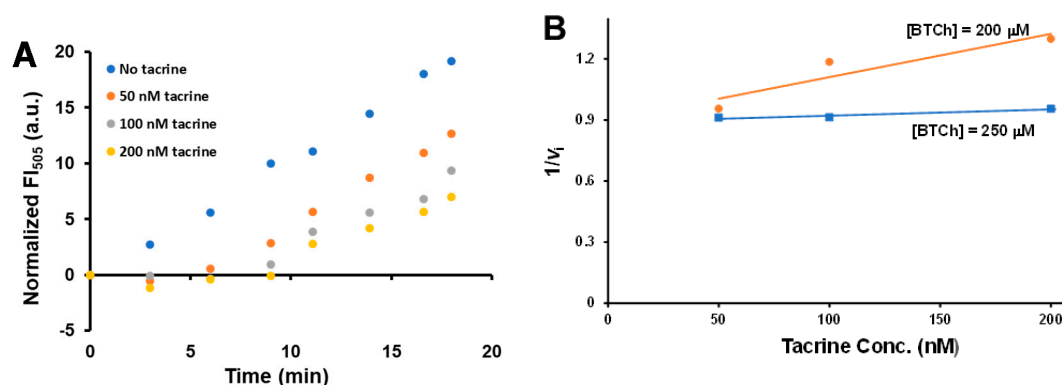


Figure 5. Tacrine inhibition on BChE catalysis analyzed by the fluorescence assay based on **11**. (A) Time-course kinetic analysis of tacrine inhibition on BChE (182.2 U L^{-1}) catalysis was performed in the presence of BTCh ($200 \mu\text{M}$) in PB. Each BChE reaction contained 0, 50, 100, or 200 nM of tacrine. (B) Dixon plot of the inhibitory kinetics of tacrine on BChE catalysis was delineated according to v_i from Figure 5A and Supplementary Materials Figure S7. The tacrine inhibitor constant K_i was determined from the minus x -axis value at which the two extrapolated lines intersected and was 5 nM in this study.

3. Materials and Methods

Except where noted all reagent-grade chemicals were purchased from commercial sources (Sigma-Aldrich (Merck Ltd., Taiwan), Acros (Geel, Belgium), Alfa Aesar (Lancashire, UK), TCI (Tokyo, Japan), and Avantor Sciences (Chu-Bei City, Taiwan) and further purified as necessary. BChE from equine serum was purchased from Sigma-Aldrich for preliminary tests. Human serum was obtained from healthy volunteers. ^1H and ^{13}C NMR spectra were recorded by using a Varian 200 or 400 MHz spectrometer (Varian, Inc., Palo Alto, CA, USA) at Kaohsiung Medical University, Taiwan (KMU). NMR samples were prepared in $(\text{CD}_3)_2\text{SO}$ or D_2O , and the chemical shifts of ^1H and ^{13}C signals were reported in parts per million based on the internal standard of each deuterated solvent. ESI high-resolution mass spectra were acquired by using APEX II Fourier-transfer mass spectrometry (FT-MS; Bruker Daltonics Inc., Taiwan) at the Department of Chemistry, National Sun Yat-Sen University, Taiwan (NSYSU-Chemistry).

3.1. Synthesis of the Key Bicyclononyne Derivatives (**6**)

3.1.1. (1R,8S,9r,Z)-Ethyl Bicyclo [6.1.0]non-4-ene-9-Carboxylate (*exo-2*) and (1R,8S,9s,Z)-Ethyl Bicyclo[6.1.0]non-4-ene-9-Carboxylate (*endo-2*)

Compounds *exo-2* and *endo-2* were synthesized according to the previously reported reaction conditions [48] but were purified by silica column chromatography procedures described below. A dichloromethane (DCM) solution (5 mL) containing **1** (2.59 g, 24 mmol) and $\text{Rh}_2(\text{OAc})_4$ (57 mg, 0.13 mmol) was placed in an ice-water bath and ethyl diazoacetate (2.4 mL, 9 mmol) was slowly added. After 40 h at room temperature (rt), the reaction was stopped by removing DCM under reduced pressure. The remaining liquid reaction mixture was loaded onto a silica column pre-equilibrated with a solution with a 1:50 ratio of diethyl ether (Et_2O) to hexane. The products were separately eluted with an Et_2O /hexane solution of 1:50 ratio. Fractions containing the desired product were pooled and evaporated under reduced pressure to obtain *exo-2* (2.41 g, 61.3%) and *endo-2* (0.78 g, 19.8%). *exo-2*: ^1H NMR (200 MHz) (CDCl_3) δ : 5.68–5.60 (m, 2H), 4.10 (q, 2H), 2.35–2.00 (m, 6H), 1.62–1.43 (m, 4H), 1.29–1.17 (m, 4H); *endo-2*: ^1H NMR (200 MHz) (CDCl_3) δ : 5.80–5.55 (m, 2H), 4.10 (q, 2H), 2.44–2.03 (m, 6H), 1.61–1.28 (m, 8H).

3.1.2. [(1*R*,4*Z*,8*S*,9*r*)-Bicyclo[6.1.0]non-4-en-9-yl]Methanol (*exo*-3), [(1*R*,4*Z*,8*S*,9*s*)-Bicyclo[6.1.0]non-4-en-9-yl]Methanol (*endo*-3), (1*R*,8*S*,9*r*)-Bicyclo[6.1.0]non-4-yn-9-ylmethanol (*exo*-4), (1*R*,8*S*,9*s*)-Bicyclo[6.1.0]non-4-yn-9-ylmethanol (*endo*-4), (1*R*,8*S*,9*r*)-Bicyclo[6.1.0]non-4-yn-9-ylmethyl (4-nitrophenyl) Carbonate (*exo*-5), and (1*R*,8*S*,9*s*)-Bicyclo[6.1.0]non-4-yn-9-ylmethyl (4-Nitrophenyl) Carbonate (*endo*-5)

Compounds 3–5 were synthesized by previously reported procedures [48].

3.1.3. [(1*R*,8*S*,9*r*)-Bicyclo[6.1.0]non-4-yn-9-yl]Methyl 2-[(2-Aminoethyl)Disulfanyl]ethyl]Carbamate (*exo*-6)

Trimethylamine (Et₃N, 4 mL) and cystamine dihydrochloride (146 mg, 0.654 mmol, 8 equiv) were added to a solution of methanol (MeOH; 16 mL), and the afforded mixture was heated at 60 °C until all of the cystamine dissolved. A solution of *exo*-5 (25 mg, 0.079 mmol, 1 equiv) in DCM (4 mL) was slowly added dropwise to the MeOH solution while stirring during a 10-min interval. The reaction was allowed to proceed at 50 °C for 15 min and was then stopped by removing the organic solvents under reduced pressure. The obtained white solid was redissolved in 20 mL of DCM and the resulting solution was extracted with 30 mL of 1 N NaOH five times and 30 mL of a saturated NaCl solution once. The final organic phase was dried over MgSO₄, filtered, and evaporated under reduced pressure to give *exo*-6 (23.6 mg, 0.072 mmol, 91%) as a yellow liquid. ¹H NMR (400 MHz) (C₂D₆OS) δ: 7.28 (quin, 1H), 3.86 (d, 2H), 3.40 (d, 2H), 2.84–2.72 (m, 6H), 2.31–2.05 (m, 7H), 1.34–1.23 (m, 3H), 0.69–0.61 (m, 3H). ¹³C NMR (100.67 MHz) (C₂D₆OS) δ: 156.4, 98.9, 67.9, 41.1, 41.0, 40.6, 37.5, 32.8, 23.4, 22.2, 20.8. HRMS (ESI) calculated for C₁₅H₂₅N₂O₂S₂, [M + H]⁺ 329.1353 (calcd), 329.1352 (found).

3.1.4. [(1*R*,8*S*,9*s*)-Bicyclo[6.1.0]non-4-yn-9-yl]Methyl 2-[(2-Aminoethyl)Disulfanyl]ethyl]Carbamate (*endo*-6)

A solution of Et₃N (4 mL) and cystamine dihydrochloride (763 mg, 3.389 mmol, 8 equiv) in MeOH (16 mL) and a solution of *endo*-5 (130 mg, 0.411 mmol, 1 equiv) in DCM (4 mL) were prepared, reacted, and worked up by following the same methods used for the synthesis of *exo*-6 described above to give the desired *endo*-6 (112 mg, 0.341 mmol, 83%) as a yellow liquid. ¹H NMR (400 MHz) (C₂D₆OS) δ: 7.29 (quin, 1H), 3.86 (d, 2H), 3.24 (d, 2H), 2.90–2.74 (m, 6H), 2.31–2.05 (m, 7H), 1.31–1.23 (m, 3H), 0.69–0.61 (m, 3H). ¹³C NMR (100.67 MHz) (C₂D₆OS) δ: 156.4, 98.9, 67.9, 37.5, 37.4, 32.8, 23.4, 22.2, 20.8. HRMS (ESI) calculated for C₁₅H₂₅N₂O₂S₂, [M + H]⁺ 329.13520 (calcd), 329.13527 (found).

3.2. Synthesis of the Azido EDANS Derivative (10)

3.2.1. 3-Azidopropanoic acid (8) and 1-[(3-Azidopropanoyl)oxy]Pyrrolidine-2,5-Dione (9)

Compounds 8 and 9 were synthesized by following the previously described methods [51].

3.2.2. 5-[[2-(3-Azidopropanamido)Ethyl]Amino]Naphthalene-1-Sulfonate (10)

EDANS (28 mg, 0.097 mmol, 1 equiv), 9 (62 mg, 0.292 mmol, 3 equiv), and *N,N*-diisopropylethylamine (DIPEA; 169.5 L, 10 equiv) were sequentially dissolved in 1 mL of dimethylformamide (DMF) to initiate the reaction, which was stirred and allowed to proceed in the dark at rt in a nitrogen atmosphere overnight. The reaction was stopped by the gradual addition of DCM to afford a yellow-white precipitate. The solid phase was filtered, washed with additional DCM, and then dissolved in MeOH in a round-bottomed flask. The resulting MeOH solution was evaporated under reduced pressure, re-dissolved in a limited volume of DCM/MeOH (20:1) solution, and loaded onto a silica column pre-equilibrated with the same solution. The products were sequentially separated by eluting with a solution of 20:1 ratio of DCM to MeOH, and then with MeOH only in the dark. Fractions containing the desired product were pooled and evaporated under reduced pressure to obtain 10 (23.8 mg, 0.065 mmol, 67.8%) as a yellow white solid. ¹H NMR (400 MHz) (D₂O) δ: 8.13 (dt, 1H), 8.08 (dd, 1H), 8.00 (d, 1H), 7.51 (q, 2H), 6.85 (d, 1H), 3.52 (t, 2H), 3.46 (t, 2H), 3.41 (t, 2H),

2.41 (t, 2H). ^{13}C NMR (100.67 MHz) (D_2O) δ : 174.0, 143.8, 138.1, 129.0, 128.3, 126.2, 124.9, 124.5, 123.6, 115.0, 106.6, 47.2, 43.0, 38.2, 35.0. HRMS (ESI) calculated for $\text{C}_{15}\text{H}_{16}\text{N}_5\text{O}_4\text{S}$, $[\text{M}-\text{H}]^-$ 362.0929 (calcd.), 362.0931 (found).

3.3. Synthesis of the EDANS–DABCYL–Paired FRET Chemical Probe (**11**)

N-Succinimidyl 4-[4-(dimethylamino)phenylazo]benzoate (26.8 mg, 0.0723 mmol, 1.2 equiv) (DABCYL NHS ester; TCI), *exo*-**6** (19.8 mg, 0.0602 mmol, 1 equiv), **10** (26.2 mg, 0.0723 mmol, 1.2 equiv), and DIPEA (68 μL , 0.3913 mmol, 6.5 equiv) were dissolved in DMF (3 mL) and stirred in the dark overnight at rt (Scheme 1). The reaction was stopped by adding 5 mL of DCM, 4 mL of 0.1 N HCl, and sufficient volume of hexane to initiate the precipitation of a black solid. After careful removal of the top aqueous solution, the remaining organic phase was refrigerated at 4 $^\circ\text{C}$ overnight, in order to promote further precipitation of the black solid. The black solid from both precipitation steps was filtered, washed with DCM, recovered from the filter paper by the addition of MeOH, and subsequently evaporated under reduced pressure to give **11** (27.1 mg, 0.0289 mmol, 48%). ^1H NMR (400 MHz) ($\text{C}_2\text{D}_6\text{OS}$) δ : 8.79 (t, 1H), 8.27 (s, 1H), 8.12–8.06 (m, 2H), 8.01–7.94 (m, 3H), 7.82–7.80 (m, 5H), 7.31–7.24 (m, 2H), 6.85 (d, 2H), 6.54–6.52 (d, 1H), 4.40 (s, 1H), 3.78 (d, 2H), 3.79–3.75 (m, 4H), 3.40 (d, 2H), 3.15–3.07 (m, 10H), 2.97–2.59 (m, 11H), 2.32–2.19 (m, 3H), 1.29–1.24 (m, 3H), 0.75–0.67 (m, 3H). ^{13}C NMR (100.67 MHz) ($\text{C}_2\text{D}_6\text{OS}$) δ : 169.6, 165.7, 156.4, 153.9, 152.9, 152.8, 144.0, 143.6, 142.5, 142.6, 134.5, 130.2, 130.5, 130.1, 128.3, 126.1, 125.2, 125.0, 124.3, 123.5, 122.8, 122.3, 121.8, 121.5, 115.9, 111.6, 102.8, 67.4, 53.4, 43.6, 43.2, 41.6, 37.7, 37.5, 37.2, 37.1, 34.2, 26.5, 25.8, 25.2, 25.1, 23.5, 21.9, 21.7, 17.9, 16.7, 12.3. HRMS (ESI) calculated for $\text{C}_{45}\text{H}_{53}\text{N}_{10}\text{O}_7\text{S}_3$, $[\text{M}-\text{H}]^-$ 941.3266 (calcd.), 941.3264 (found).

3.4. Synthesis of the GSH Derivatives, **12** and **13**

3.4.1. Methyl

(2*S*)-2-Amino-5-((2*R*)-1-[(2-Ethoxy-2-Oxoethyl)Amino]-1-oxo-3-Sulfanylpropan-2-yl)Amino)-5-Oxopentanoic Acid (**12**)

The reaction mixture was prepared by transfer of 96% sulfuric acid (204 μL , 3.675 mmol, 7.5 equiv) to ethanol (EtOH, 5 mL) submerged in an ice-water bath, followed by addition of GSH (150 mg, 0.489 mmol, 1 equiv) to the EtOH solution while stirring. The ice-water bath was immediately removed from the reaction to promote complete dissolution of GSH in the EtOH solution. Anhydrous Mg_2SO_4 (0.5 g) was then added to the afforded GSH solution in EtOH to begin the reaction at rt, for 7 h, with stirring. The final reaction mixture was filtered to remove MgSO_4 , placed in an ice-water bath, and followed by adding cold Et_2O (50 mL). The final solution was continuously immersed in the ice-water bath for 1 h, in order to obtain precipitates after filtration. The crude precipitate was washed with cold Et_2O and then evaporated under reduced pressure, to afford **12** (140.9 mg, 0.42 mmol, 86%) as a white solid. ^1H NMR (400 MHz) ($\text{C}_2\text{D}_6\text{OS}$) δ : 8.47 (m, 1H), 8.20 (m, 1H), 4.39 (m, 1H), 4.20 (q, 1H), 4.09 (m, 2H), 3.81 (m, 2H), 3.73 (q, 4H), 2.80 (m, 1H), 2.67 (m, 1H), 2.33 (m, 2H), 2.00 (m, 2H), 1.24 (t, 1H), 1.17 (t, 3H). ^{13}C NMR (100.67 MHz) ($\text{C}_2\text{D}_6\text{OS}$) δ : 170.9, 170.5, 170.4, 169.7, 61.3, 60.6, 55.0, 51.7, 40.9, 30.8, 26.2, 14.1. HRMS (ESI) calculated for $\text{C}_{12}\text{H}_{22}\text{N}_3\text{O}_6\text{S}$, $[\text{M} + \text{H}]^+$ 336.12238 (calcd.), 336.12242 (found).

3.4.2. (2*S*)-2-Amino-5-((2*R*)-1-[(2-Methoxy-2-Oxoethyl)Amino]-1-oxo-3-Sulfanylpropan-2-yl)Amino)-5-Oxopentanoate (**13**)

Compound **13** was synthesized according to a published method [54].

3.5. Spectroscopic Measurements

UV–Vis absorption spectra were recorded on an Amersham Biosciences Ultrospec 2100 pro spectrophotometer (KMU) and fluorescence spectra were obtained with a PerkinElmer LS-55 fluorescence spectrometer (KMU) with the settings of the excitation wavelength at 336 nm for EDANS detection in a 1 cm standard quartz cuvette.

3.6. Specificity and Mechanism of the FRET Chemical Probe **11** Reactions with Thiols

The propensity of **11** to preferentially react with certain compounds was characterized by analyzing k_1 for the reactions. The determination of k_1 for each reaction was based on the measurement of the release of the EDANS fluorescence ($\lambda_{\max} = 505$ nm) in the presence of a reactant in significant molar excess relative to that of **11** during the course of the reaction. The procedure is briefly described below. A quartz cuvette was partially filled with 1.125 mL of phosphate buffer (PB, pH = 7.4, 0.1 M) and mounted onto the temperature controller of the PerkinElmer LS-55 fluorescence spectrometer. Three hundred microliters of a 250 mM solution of one of the reactants (DL-dithiothreitol (DTT), L-glutamate, glycine, L-cysteine, GSH, L-serine, L-lysine, L-methionine, 2-mercaptoethanol, and 2-aminoethanethiol) in PB and 75 μ L of **11** (500 μ M in DMF) were then sequentially transferred to the PB solution in the cuvette for the final concentrations of 50 mM and 25 μ M, respectively, and to initiate the reaction. Progress of the reaction at 25 °C was monitored by measuring the EDANS fluorescence until signal saturation occurred, which required a reaction interval of 15–90 min and depended on the reactivity of each compound. The normalized FL intensity data at 505 nm were acquired by subtracting a background FL₅₀₅ intensity of **11** from the original FL₅₀₅ intensity measurement. The normalized data were fitted to a single-exponential equation for first-order kinetics $F(t) = F_0 + F_{\max}(1 - e^{-k_1 t})$ [$F(t)$, normalized EDANS fluorescence at a specific time point t] to afford k_1 (GraphPad, La Jolla, CA, USA). Similar kinetic analysis was employed to determine k_2 in which the concentration of DTT in the reaction was 10, 25, 50, 75, 100, 125, or 150 mM. A k_2 value was acquired from the slope of a linear regression curve derived from a plot of k_1 vs. [DTT]. The pH dependency in the reaction of **11** with DTT was studied by the same first-order kinetics in the presence of different pH buffers, including MES (pH 5.5–6.5), PIPES (pH 6.5–7.5), EPPS (pH 7.5–8.6), and CHES (pH 8.6–9.5). The pH titration results provided the pK_{a1} value of DTT according to the equation $k_1 = k_{1,\max}[1 + 10^{(pK_{a1} - pH)}]$ (GraphPad, USA). The similar k_1 analysis on the **11**-DTT reaction was also exploited to unveil effects of 1 mM of metal ions (K^+ , Li^+ , Na^+ , Ca^{2+} , Cd^{2+} , $Co(II)$, $Cu(II)$, Mg^{2+} , $Mn(II)$, $Ni(II)$, Zn^{2+} , $Fe(III)$; chloride salts) on the reaction. The ability of **11** to discriminate against GSH was likewise explicated by first-order kinetics of the reactions between **11** and 50 mM of one of the GSH derivatives, **12** and **13**. The kinetic experiments with each reactant for the determination of k_1 were performed in quadruplicate; the reported k_1 was the mean \pm SD of the four experiments.

3.7. The **11**-Based Assay for Fluorescence Turn-On Analysis of BChE Activity in Serum and in the Presence of a BChE Inhibitor

Compound **11**-based analysis of BChE activity was performed qualitatively in vials and quantitatively in the fluorescence spectrometer. In the vial assay, five different solutions were prepared by different combinations of 50 μ M of **11**, 5 mM of *S*-butyrylthiocholine iodide (BTCh), 182.2 U L⁻¹ of BChE, or 50 μ M of GSH in PB. The solutions were prepared in the dark, in five different vials, and the reactions were allowed to proceed at rt in the dark for 90 min. The resulting fluorescence was visualized and photographed by the illumination of the 365 nm light from a hand-held lamp.

Quantitative measurements of BChE activity by the **11**-based assay in the fluorescence spectrometer are briefly described below. A solution of **11** (25 μ M), BChE (1.82–182.2 U L⁻¹), and BTCh (5 mM) in PB was prepared in a quartz cuvette previously mounted onto the temperature controller of the PerkinElmer LS-55 fluorescence spectrometer. BChE catalysis was carried out at 37 °C for 90 min; reaction progression was monitored by the FL intensity at 505 nm as a function of reaction time. The normalized FL intensity data at 505 nm were acquired by subtracting a background FL₅₀₅ intensity of **11** from the original FL₅₀₅ intensity reading. The FL changes in windows of the steady state reactions were used to calculate the initial rate (v_i) of BChE catalysis. For measurements of BChE activity in blood samples, a trained phlebotomist at KMU Hospital obtained 20 mL of whole blood samples from three healthy male volunteers. A 10-fold dilution of the blood sample was used to substitute for BChE in the **11**-based assay. Finally, effects of the inhibitor tacrine on BChE catalysis were studied by the **11**-based analysis in which each reaction contained **11** (25 μ M), BChE (182.2 U L⁻¹), BTCh (250 or

200 μM), and tacrine (50, 100, or 200 nM) in PB. Each specific BChE catalysis was performed three times with the reported v_1 as a mean \pm SD of the experiments. BChE catalysis, in the presence of not only the reactants in PB described above but also of GSH (10 μM , 50 μM , or 50 mM), was similarly studied to acquire the corresponding $v_1 \pm$ SD.

4. Conclusions

We have synthesized the novel FRET chemical probe **11** and established an **11**-based quantitative method for the direct and accurate measurement of BChE activity in serum, while selectively discriminating between GSH and the products of BChE catalysis. Moreover, the BChE activity assay based on **11** provides a platform for screening of BChE inhibitors useful to the treatment of human diseases such as Alzheimer's. We are developing **11**-based high-throughput analysis for diagnosing aberrant BChE activity in serum and other biological samples from patients. In addition, the trifunctional characteristics of the bicyclononynes **6** enable a facile, one-pot reaction approach to modulated synthesis of diverse bioconjugates and chemical probes similar to **11**. These chemical probes could provide LOD and linear detection range superior to that of **11** utilized in the current assay for BChE activity. Lastly, in comparison with nanoprobe-based bioassays, fluorescent chemical probes such as **11** are generally more biocompatible and nontoxic to biological systems. Fluorescent chemical probes like **11** clearly have the significant advantage over nanoprobe when the probes are administered to cells in order to perform ex vivo or in vivo analysis. Therefore, in addition to the assay for BChE activity, the fluorescent chemical probe **11** could have broader biomedical and scientific applications than those of nanoprobe. We are currently expanding the **11** studies to meet these expectations.

Supplementary Materials: The following are available online at <http://www.mdpi.com/2073-4344/10/10/1169/s1>. Scheme S1: Synthesis of the key bicyclononyne derivatives (**6**). Scheme S2: Obliteration of the FRET effect in **11** and release of the EDANS fluorescence initiated by nucleophilic attack of **11** by thiolates (highlighted in pink in Scheme 1 and here). Figure S1: The UV-Vis spectra for 50 μM of the FRET probe **11** (-, the blue curve), EDANS (-, the red curve), and DABCYL (-, the green curve) in phosphate buffered saline (PBS). Figure S2: Visualization of the EDANS fluorescence to explore the properties of the fluorescent emission from **11** in the presence of various reactants. Figure S3: Pseudo-first-order reactions of **11** (25 μM) with 50 mM of (A) DTT, (B) GSH, (C) L-cysteine, (D) 2-mercaptoethanol, (E) 2-aminoethanethiol, or (F) five non-thiol amino acids (L-methionine, L-lysine, L-serine, L-glutamate, and glycine) in PB. Figure S4: Effects of metal ion (1 mM) on the pseudo-first-order reactions of **11** (25 μM) with 50 mM DTT in PB. Figure S5: Kinetic analysis of the pseudo-first-order reactions of **11** (25 μM) with 50 mM of one of the structure-modified GSH derivatives **12** and **13** in PB. Figure S6: Presence of 50 μM or 50 mM of GSH in the BChE-BTCh-**11** reaction did not affect release of the EDANS fluorescence. Figure S7: Tacrine inhibition on BChE catalysis analyzed by the fluorescence assay based on **11**. Table S1: Comparison on analytical performance of optical assays for BChE activity quantification, NMR, and HRMS spectra for compounds (**6**, **10**, **11**, and **12**).

Author Contributions: Conceptualization, T.-P.W.; methodology, T.-P.W., M.-M.G., C.-Y.D., S.S., and C.-C.H.; validation, M.-M.G., C.-C.H., and B.-K.F.; formal analysis, T.-P.W. and M.-M.G.; investigation, M.-M.G., B.-K.F., H.-B.L., and C.-H.H.; resources, C.-Y.D., C.-C.H., C.-W.O., J.-J.W., and P.-L.L.; data curation, T.-P.W., M.-M.G., and B.-K.F.; writing—original draft preparation, T.-P.W., M.-M.G., and S.S.; writing—review and editing, T.-P.W., C.-Y.D., S.S., and C.-W.O.; visualization, T.-P.W.; supervision, T.-P.W.; project administration, T.-P.W.; funding acquisition, T.-P.W. and C.-W.O. All authors have read and agreed to the published version of the manuscript.

Funding: This research was funded by the Ministry of Science and Technology of Taiwan (MOST 104-2113-M-037-013- and 106-2113-M-037-010-) and the Kaohsiung Medical University Research Foundation (KMU-M106015 and KMU-M108018) awarded to T.-P.W., and from NSYSU-KMU JOINT RESEARCH PROJECT (#NSYSUKMU 109- P018) awarded to C.-W.O. and T.-P.W.

Acknowledgments: We thank Susan Fetzter for critically reading the manuscript. We also thank the Center for Research Resources and Development of KMU for technical and instrumental assistance.

Conflicts of Interest: The authors declare no conflict of interest. The funders had no role in the design of the study; in the collection, analyses, or interpretation of data; in the writing of the manuscript; or in the decision to publish the results.

Abbreviations

AChE	acetylcholinesterase
BChE	butyrylcholinesterase
BTCh	S-butyrylthiocholine iodide
ChE	cholinesterase
CHES	2-(cyclohexylamino)ethanesulfonic acid
DABCYL	4-[4-(dimethylamino)phenylazo]benzoic acid
DABCYL NHS ester	N-succinimidyl 4-[4-(dimethylamino)phenylazo]benzoate
DCM	dichloromethane
DIPEA	N,N-diisopropylethylamine
DMF	dimethylformamide
DTNB	5'-dithiobis(2-nitrobenzoic acid)
DTT	DL-dithiothreitol
EDANS	5-(2-aminoethylamino)-1-naphthalenesulfonic acid
EPPS	4-(2-hydroxyethyl)-1-piperazinepropanesulfonic acid
Et ₃ N	trimethylamine
Et ₂ O	diethyl ether
EtOH	ethanol
FRET	fluorescence resonance energy transfer
FT-MS	Fourier-transfer mass spectrometry
GSH	glutathione
LOD	limit of detection
MeOH	methanol
MES	2-(N-morpholino)ethanesulfonic acid
PB	phosphate buffer
PBS	phosphate buffered saline
PIPES	1,4-piperazinediethanesulfonic acid
SPAAC	strained-promoted azide-alkyne cycloaddition
TCh	thiocholine

References

- Lockridge, O. Review of human butyrylcholinesterase structure, function, genetic variants, history of use in the clinic, and potential therapeutic uses. *Pharmacol. Ther.* **2015**, *148*, 34–46. [[CrossRef](#)] [[PubMed](#)]
- Pope, C.N.; Brimijoin, S. Cholinesterases and the fine line between poison and remedy. *Biochem. Pharmacol.* **2018**, *153*, 205–216. [[CrossRef](#)] [[PubMed](#)]
- Chen, P.V.; Gao, Y.; Geng, L.; Brimijoin, S. Butyrylcholinesterase gene transfer in obese mice prevents postdieting body weight rebound by suppressing ghrelin signaling. *Proc. Natl. Acad. Sci. USA* **2017**, *114*, 10960–10965. [[CrossRef](#)]
- Poetsch, N.; Sturdza, A.; Aust, S.; Polterauer, S.; Grimm, C.; Schwameis, R.; Pötter, R.; Koelbl, H.; Reinthaller, A.; Seebacher, V. The value of pretreatment serum butyrylcholinesterase level as a novel prognostic biomarker in patients with cervical cancer treated with primary (chemo-)radiation therapy. *Strahlenther. Onkol.* **2019**, *195*, 430–440. [[CrossRef](#)]
- Zivkovic, A.R.; Schmidt, K.; Stein, T.; Münzberg, M.; Brenner, T.; Weigand, M.A.; Kleinschmidt, S.; Hofer, S. Bedside-measurement of serum cholinesterase activity predicts patient morbidity and length of the intensive care unit stay following major traumatic injury. *Sci. Rep.* **2019**, *9*, 10437. [[CrossRef](#)]
- Darvesh, S.; Hopkins, D.A.; Geula, C. Neurobiology of butyrylcholinesterase. *Nat. Rev. Neurosci.* **2003**, *4*, 131–138. [[CrossRef](#)]
- Santarpia, L.; Grandone, I.; Contaldo, F.; Pasanisi, F. Butyrylcholinesterase as a prognostic marker: A review of the literature. *J. Cachex Sarcopenia Muscle* **2012**, *4*, 31–39. [[CrossRef](#)]
- Klocker, E.V.; Barth, D.A.; Riedl, J.M.; Prinz, F.; Szkandera, J.; Schlick, K.; Kornprat, P.; Lackner, C.; Lindenmann, J.; Stoeger, H.; et al. Decreased Activity of Circulating Butyrylcholinesterase in Blood Is an Independent Prognostic Marker in Pancreatic Cancer Patients. *Cancers* **2020**, *12*, 1154. [[CrossRef](#)]

9. Chen, G.; Feng, H.; Jiang, X.; Xu, J.; Pan, S.; Qian, Z. Redox-Controlled Fluorescent Nanoswitch Based on Reversible Disulfide and Its Application in Butyrylcholinesterase Activity Assay. *Anal. Chem.* **2018**, *90*, 1643–1651. [[CrossRef](#)]
10. Meden, A.; Knez, D.; Jukič, M.; Brazzolotto, X.; Gršič, M.; Pišlar, A.; Zahirović, A.; Kos, J.; Nachon, F.; Svete, J.; et al. Tryptophan-derived butyrylcholinesterase inhibitors as promising leads against Alzheimer's disease. *Chem. Commun.* **2019**, *55*, 3765–3768. [[CrossRef](#)]
11. Zhou, S.; Yuan, Y.; Zheng, F.; Zhan, C.-G. Structure-based virtual screening leading to discovery of highly selective butyrylcholinesterase inhibitors with solanaceous alkaloid scaffolds. *Chem. Interact.* **2019**, *308*, 372–376. [[CrossRef](#)]
12. Jing, L.; Wu, G.; Kang, D.; Zhou, Z.; Song, Y.; Liu, X.; Zhan, P. Contemporary medicinal-chemistry strategies for the discovery of selective butyrylcholinesterase inhibitors. *Drug Discov. Today* **2019**, *24*, 629–635. [[CrossRef](#)] [[PubMed](#)]
13. Li, Q.; Yang, H.; Chen, Y.; Sun, H. Recent progress in the identification of selective butyrylcholinesterase inhibitors for Alzheimer's disease. *Eur. J. Med. Chem.* **2017**, *132*, 294–309. [[CrossRef](#)] [[PubMed](#)]
14. Pajk, S.; Knez, D.; Košak, U.; Zorović, M.; Brazzolotto, X.; Coquelle, N.; Nachon, F.; Colletier, J.-P.; Živin, M.; Stojan, J.; et al. Development of potent reversible selective inhibitors of butyrylcholinesterase as fluorescent probes. *J. Enzym. Inhib. Med. Chem.* **2020**, *35*, 498–505. [[CrossRef](#)] [[PubMed](#)]
15. Liu, S.; Xiong, H.; Yang, J.-Q.; Yang, S.-H.; Li, Y.; Yang, W.; Yang, G.-F. Discovery of Butyrylcholinesterase-Activated Near-Infrared Fluorogenic Probe for Live-Cell and In Vivo Imaging. *ACS Sens.* **2018**, *3*, 2118–2128. [[CrossRef](#)]
16. Seo, M.; Yamada, T.; Tamaki, S.; Hikoso, S.; Yasumura, Y.; Higuchi, Y.; Nakagawa, Y.; Uematsu, M.; Abe, H.; Fujii, H.; et al. Prognostic Significance of Serum Cholinesterase Level in Patients With Acute Decompensated Heart Failure With Preserved Ejection Fraction: Insights From the PURSUIT-HFpEF Registry. *J. Am. Hear. Assoc.* **2020**, *9*, 014100. [[CrossRef](#)] [[PubMed](#)]
17. Cerasoli, D.M.; Armstrong, S.J.; Reeves, T.E.; Hodgins, S.M.; Kasten, S.A.; Lee-Stubbs, R.B.; Cadieux, C.L.; Otto, T.C.; Capacio, B.R.; Lenz, D.E. Butyrylcholinesterase, a stereospecific in vivo bioscavenger against nerve agent intoxication. *Biochem. Pharmacol.* **2019**, *171*, 113670. [[CrossRef](#)]
18. Vallianou, N.G.; Evangelopoulos, A.; Bountziouka, V.; Bonou, M.; Katsagoni, C.; Vogiatzakis, E.D.; Avgerinos, P.C.; Barbetseas, J.; Panagiotakos, D.B.; Katsagoni, C. Association of butyrylcholinesterase with cardiometabolic risk factors among apparently healthy adults. *J. Cardiovasc. Med.* **2014**, *15*, 377–383. [[CrossRef](#)]
19. Adam, E.H.; Haas, V.; Lindau, S.; Zacharowski, K.; Scheller, B. Cholinesterase alterations in delirium after cardiac surgery: A German monocentric prospective study. *BMJ Open* **2020**, *10*, e031212. [[CrossRef](#)]
20. Pohanka, M. Butyrylcholinesterase as a biochemical marker. *Bratisl. Lek. List.* **2013**, *114*, 726–734. [[CrossRef](#)]
21. Reed, B.A.; Sabourin, C.L.; Lenz, D.E. Human butyrylcholinesterase efficacy against nerve agent exposure. *J. Biochem. Mol. Toxicol.* **2017**, *31*, e21886. [[CrossRef](#)] [[PubMed](#)]
22. Lockridge, O.; Norgren, R.B., Jr.; Johnson, R.C.; Blake, T.A. Naturally Occurring Genetic Variants of Human Acetylcholinesterase and Butyrylcholinesterase and Their Potential Impact on the Risk of Toxicity from Cholinesterase Inhibitors. *Chem. Res. Toxicol.* **2016**, *29*, 1381–1392. [[CrossRef](#)] [[PubMed](#)]
23. Zhao, B.; Ni, Y.; Tian, X. Low Plasma Cholinesterase Activity is Associated with Postoperative Delirium After Noncardiac Surgery in Elderly Patients: A Prospective Observational Study. *J. Psychosom. Res.* **2019**, *60*, 190–196. [[CrossRef](#)] [[PubMed](#)]
24. Anjum, A.; Biswas, S.; Rahman, M.; Rahman, A.; Siddique, A.E.; Karim, Y.; Aktar, S.; Nikkon, F.; Haque, A.; Himeno, S.; et al. Butyrylcholinesterase—A potential plasma biomarker in manganese-induced neurobehavioral changes. *Environ. Sci. Pollut. Res.* **2019**, *26*, 6378–6387. [[CrossRef](#)] [[PubMed](#)]
25. Miao, Y.; He, N.; Zhu, J.-J. History and New Developments of Assays for Cholinesterase Activity and Inhibition. *Chem. Rev.* **2010**, *110*, 5216–5234. [[CrossRef](#)] [[PubMed](#)]
26. Pohanka, M. Voltammetric assay of butyrylcholinesterase in plasma samples and its comparison to the standard spectrophotometric test. *Talanta* **2014**, *119*, 412–416. [[CrossRef](#)] [[PubMed](#)]
27. Ding, J.; Qin, W. Potentiometric sensing of butyrylcholinesterase based on in situ generation and detection of substrates. *Chem. Commun.* **2009**, 971–973. [[CrossRef](#)]

28. El-Rahman, M.K.A.; Eid, S.M.; Elghobashy, M.R.; Kelani, K.M. Inline potentiometric monitoring of Butyrylcholinesterase activity based on metabolism of bambuterol at the point of care. *Sens. Actuators B Chem.* **2019**, *285*, 216–223. [[CrossRef](#)]
29. Wang, L.; Du, D.; Lu, D.; Lin, C.-T.; Smith, J.N.; Timchalk, C.; Liu, F.; Wang, J.; Lin, Y. Enzyme-linked immunosorbent assay for detection of organophosphorylated butyrylcholinesterase: A biomarker of exposure to organophosphate agents. *Anal. Chim. Acta* **2011**, *693*, 1–6. [[CrossRef](#)] [[PubMed](#)]
30. Yang, Y.; Liu, H.; Chen, Z.; Wu, T.; Jiang, Z.; Tong, L.; Tang, B. A Simple 3D-Printed Enzyme Reactor Paper Spray Mass Spectrometry Platform for Detecting BuChE Activity in Human Serum. *Anal. Chem.* **2019**, *91*, 12874–12881. [[CrossRef](#)] [[PubMed](#)]
31. Jońca, J.; Żuk, M.; Wasąg, B.; Janaszak-Jasiecka, A.; Lewandowski, K.; Wielgomas, B.; Waleron, K.; Jasiecki, J. New Insights into Butyrylcholinesterase Activity Assay: Serum Dilution Factor as a Crucial Parameter. *PLoS ONE* **2015**, *10*, e0139480. [[CrossRef](#)]
32. Ellman, G.L.; Courtney, K.; Andres, V.; Featherstone, R.M. A new and rapid colorimetric determination of acetylcholinesterase activity. *Biochem. Pharmacol.* **1961**, *7*, 88–95. [[CrossRef](#)]
33. Jones, D.P.; Carlson, J.L.; Samiec, P.S.; Sternberg, P.; Mody, V.C.; Reed, R.L.; Brown, L.A.S. Glutathione measurement in human plasma. *Clin. Chim. Acta* **1998**, *275*, 175–184. [[CrossRef](#)]
34. Pohanka, M.; Drtinova, L. Spectrophotometric methods based on 2,6-dichloroindophenol acetate and indoxylacetate for butyrylcholinesterase activity assay in plasma. *Talanta* **2013**, *106*, 281–285. [[CrossRef](#)] [[PubMed](#)]
35. Bagheri, N.; Cinti, S.; Caratelli, V.; Massoud, R.; Saraji, M.; Moscone, D.; Arduini, F. A 96-well wax printed Prussian Blue paper for the visual determination of cholinesterase activity in human serum. *Biosens. Bioelectron.* **2019**, *134*, 97–102. [[CrossRef](#)]
36. Lu, L.; Xia, Y. Enzymatic Reaction Modulated Gold Nanorod End-to-End Self-Assembly for Ultrahigh Sensitively Colorimetric Sensing of Cholinesterase and Organophosphate Pesticides in Human Blood. *Anal. Chem.* **2015**, *87*, 8584–8591. [[CrossRef](#)]
37. Li, P.Y.; Chen, Y.; Chen, C.H.; Liu, Y. Multi-charged bis(p-calixarene)/pillararene functionalized gold nanoparticles for ultra-sensitive sensing of butyrylcholinesterase. *Soft Matter* **2019**, *15*, 8197–8200. [[CrossRef](#)]
38. Guilbault, G.G.; Kramer, D.N. Resorufin Butyrate and Indoxyl Acetate as Fluorogenic Substrates for Cholinesterase. *Anal. Chem.* **1965**, *37*, 120–123. [[CrossRef](#)]
39. Kang, S.; Yang, W.; Oh, J.; Lee, S.; Seo, J. A direct assay of butyrylcholinesterase activity using a fluorescent substrate. *Org. Biomol. Chem.* **2016**, *14*, 8815–8820. [[CrossRef](#)]
40. Yang, S.-H.; Sun, Q.; Xiong, H.; Liu, S.; Moosavi, B.; Yang, W.-C.; Yang, G.-F. Discovery of a butyrylcholinesterase-specific probe via a structure-based design strategy. *Chem. Commun.* **2017**, *53*, 3952–3955. [[CrossRef](#)]
41. Yoo, S.; Oh, J. A fluorescent probe for butyrylcholinesterase activity in human serum based on a fluorophore with specific binding affinity for human serum albumin. *Chem. Commun.* **2019**, *55*, 14574–14577. [[CrossRef](#)] [[PubMed](#)]
42. Chen, G.; Feng, H.; Xi, W.; Xu, J.; Pan, S.; Qian, Z. Thiol–ene click reaction-induced fluorescence enhancement by altering the radiative rate for assaying butyrylcholinesterase activity. *Analyst* **2019**, *144*, 559–566. [[CrossRef](#)] [[PubMed](#)]
43. Yuan, X.; Chen, S.; Li, S.; Liu, Q.; Kou, M.; Xu, T.; Luo, H.; Huang, K.; Zhang, M. Enzymatic reaction modulation of G-quadruplex formation for the sensitive homogeneous fluorescence sensing of cholinesterase and organophosphate pesticides. *Anal. Methods* **2019**, *11*, 980–988. [[CrossRef](#)]
44. Deng, W.; Chen, P.; Hu, P.; He, Z.; Zhang, M.; Yuan, X.; Huang, K. Enzymatic reaction modulated synthesis of quantum dots for visual detection of cholinesterase activity and inhibitor. *Sens. Actuators B Chem.* **2019**, *292*, 180–186. [[CrossRef](#)]
45. Xu, X.; Cen, Y.; Xu, G.; Wei, F.; Shi, M.; Hu, Q. A ratiometric fluorescence probe based on carbon dots for discriminative and highly sensitive detection of acetylcholinesterase and butyrylcholinesterase in human whole blood. *Biosens. Bioelectron.* **2019**, *131*, 232–236. [[CrossRef](#)]
46. Zhang, X.-P.; Zhao, C.-X.; Shu, Y.; Wang, J. Gold Nanoclusters/Iron Oxyhydroxide Platform for Ultrasensitive Detection of Butyrylcholinesterase. *Anal. Chem.* **2019**, *91*, 15866–15872. [[CrossRef](#)]

47. Li, T.; Gao, Y.; Li, H.; Zhang, C.; Xing, Y.; Jiao, M.; Shi, Y.-E.; Li, W.; Zhai, Y.; Wang, Z.; et al. Ultrasensitive detection of butyrylcholinesterase activity based on the inner filter effect of MnO₂ nanosheets on sulfur nanodots. *Analyst* **2020**, *145*, 5206–5212. [[CrossRef](#)]
48. Dommerholt, J.; Schmidt, S.; Temming, R.; Hendriks, L.J.A.; Rutjes, F.P.J.T.; Van Hest, J.C.M.; Lefebber, D.J.; Friedl, P.; Van Delft, F.L. Readily Accessible Bicyclononynes for Bioorthogonal Labeling and Three-Dimensional Imaging of Living Cells. *Angew. Chem. Int. Ed.* **2010**, *49*, 9422–9425. [[CrossRef](#)]
49. Clegg, R.M.; Murchie, A.I.H.; Zechel, A.; Carlberg, C.; Diekmann, S.; Lilley, D.M.J. Fluorescence resonance energy transfer analysis of the structure of the four-way DNA junction. *Biochemistry* **1992**, *31*, 4846–4856. [[CrossRef](#)]
50. Piggott, A.M.; Karuso, P. Fluorometric Assay for the Determination of Glutathione Reductase Activity. *Anal. Chem.* **2007**, *79*, 8769–8773. [[CrossRef](#)]
51. Su, Y.-C.; Lo, Y.-L.; Hwang, C.-C.; Wang, L.-F.; Wu, M.H.; Wang, E.-C.; Wang, Y.-M.; Wang, T.-P. Azide–alkyne cycloaddition for universal post-synthetic modifications of nucleic acids and effective synthesis of bioactive nucleic acid conjugates. *Org. Biomol. Chem.* **2014**, *12*, 6624–6633. [[CrossRef](#)] [[PubMed](#)]
52. Su, Y.-C.; Chen, H.-Y.; Ko, N.C.; Hwang, C.-C.; Wu, M.H.; Wang, L.-F.; Wang, Y.-M.; Chang, S.-N.; Wang, E.-C.; Wang, T.-P. Effective and site-specific phosphoramidation reaction for universally labeling nucleic acids. *Anal. Biochem.* **2014**, *449*, 118–128. [[CrossRef](#)] [[PubMed](#)]
53. Lukesh, I.J.C.; Wallin, K.K.; Raines, R.T. Pyrazine-derived disulfide-reducing agent for chemical biology. *Chem. Commun.* **2014**, *50*, 9591–9594. [[CrossRef](#)]
54. MirzaHosseini, A.; Somlyay, M.; Noszál, B. The comprehensive acid–base characterization of glutathione. *Chem. Phys. Lett.* **2015**, *622*, 50–56. [[CrossRef](#)]



© 2020 by the authors. Licensee MDPI, Basel, Switzerland. This article is an open access article distributed under the terms and conditions of the Creative Commons Attribution (CC BY) license (<http://creativecommons.org/licenses/by/4.0/>).